



Published in final edited form as:

Neuroimage. 2010 February 15; 49(4): 3122–3131. doi:10.1016/j.neuroimage.2009.11.005.

***In vivo* visualization of reactive gliosis using manganese-enhanced magnetic resonance imaging**

Yuko Kawai^a, Ichio Aoki^{b,*}, Masahiro Umeda^c, Toshihiro Higuchi^a, Jeff Kershaw^b, Makoto Higuchi^b, Afonso C. Silva^d, and Chuzo Tanaka^{a,c}

^aDepartment of Neurosurgery, Meiji University of Integrative Medicine, Kyoto, 629-0392, Japan

^bMolecular Imaging Center, National Institute of Radiological Sciences, Anagawa 4-9-1, Inage, Chiba, 263-8555, Japan

^cDepartment of Medical Informatics, Meiji University of Integrative Medicine, Kyoto, 629-0392, Japan

^dCerebral Microcirculation Unit, Laboratory of Functional and Molecular Imaging, National Institute of Neurological Disorders and Stroke, National Institutes of Health, Bethesda, MD 20892-1065, USA

Abstract

Reactive astrogliosis occurs after diverse central nervous system (CNS) insults. While astrogliosis provides protection against inflammation, it is also obstructive in the progress of neuranogenesis after CNS insults. Thus, a method that enables *in vivo* visualization and tissue characterization for gliosis would be invaluable for studies of CNS insults and corresponding treatments. Manganese has proven to be a useful MRI contrast agent that enters cells via Ca²⁺ channels and has been applied to manganese-enhanced MRI (MEMRI) for neuronal functional mapping. This study investigated whether MEMRI can detect astrogliosis after focal ischemia *in vivo*. Rats were divided into groups according to the number of days after either transient middle cerebral artery occlusion or a sham. Ring- or crescent-shaped enhancement of MEMRI corresponded to the GFAP-positive astroglia observed in the peripheral region of the ischemic core 11 days after middle cerebral artery occlusion. This indicates that MEMRI enhancement predominantly reflects reactive astrogliosis after stroke.

Keywords

Reactive gliosis; Stroke; Brain ischemia; Manganese; MEMRI; MRI

Introduction

Astroglia turn ‘reactive’ in response to diverse central nervous system (CNS) insults (Perry and Andersson, 1992; Sofroniew, 2005). Reactive gliosis predominantly results from the

*Corresponding author. Fax: +81 43 206 3276. aoki@nirs.go.jp (I. Aoki).

Competing interests statement

The authors have no competing interests to declare.

proliferation and enlargement of astroglia after diverse insults to the CNS. Recently, the multiple roles of reactive astroglia in CNS insults have been documented using transgenic manipulations. The scar-forming properties of reactive astroglia have been shown to have a protective role against inflammation (Giulian, 1993). Also, the ablation of scar formation after CNS insults in transgenic mice showed that reactive astroglia have an important role in the regulation of inflammation after CNS injury (Bush et al., 1999; Faulkner et al., 2004). Although the mechanism underlying the regulatory role of reactive astroglia remains unclear, it has been demonstrated in animal models that several factors, such as the modulation of leukocyte entry (John et al., 2003) and transcription 3 signaling (Okada et al., 2006), are involved.

On the other hand, gliosis and the formation of glial scarring are regarded as a major obstacle to axonal regeneration after CNS injury, and therefore, regulation of the gliosis is an important issue for neuranagenic therapy. Ablation of reactive astroglia in mice leads to increased nerve fiber growth in the immediate vicinity of CNS injuries such as GFAP/vimentin deficient (Menet et al., 2003) or EphA4 gene knockout models (Goldshmit et al., 2004). Recently, it has also been recognized that cells of the mononuclear phagocyte lineage, macrophages and microglia, contribute to gliosis (Perry and Andersson, 1992) and link with astroglia inextricably through cytokine, which is a low-molecular weight glycoprotein (John et al., 2003; Norenberg, 1994). Therefore, controlling the time course of reactive gliosis and the suppression of inflammation are keys to the treatment of CNS insults, and *in vivo* visualization and tissue characterization for reactive gliosis are needed not only for studies of CNS disturbance and neuranagenesis but also for optimization of safer regeneration therapy.

Manganese chloride ($MnCl_2$) has been shown to be a positive MRI contrast agent. The MRI signal intensity is altered due more to changes in T_1 (longitudinal relaxation time) than T_2 (transverse relaxation time), thus providing increased signal in T_1 -weighted MRI (Mendonca et al., 1983). Mn^{2+} is an essential heavy metal and can enter cells via voltage-gated calcium ion (Ca^{2+}) channels (Hunter et al., 1980; Narita et al., 1990) enabling the visualization of neuronal activity (Lin and Koretsky, 1997) and neuro- and cytoarchitecture (Aoki et al., 2004; Watanabe et al., 2002). The unique biological properties of Mn^{2+} have generated renewed interest in exploring the potential of this agent as an MRI contrast agent with manganese-enhanced MRI (MEMRI).

It is known that Mn is needed for glutamine synthetase in astroglia (Carl et al., 1993) and it is also a cofactor of the mitochondrial form of superoxide dismutase (Sugaya et al., 1997). Astroglia act as “metal depots” (Tiffany-Castiglione and Qian, 2001) and there is a lot of evidence for a relationship between Mn and astroglia. Around 80% of Mn in the brain is associated with glutamine synthetase (Wedler and Denman, 1984), which is located primarily in astroglia *in vivo* as assessed using ultrastructural immunocytochemistry (Norenberg and Martinez-Hernandez, 1979). Mn administered via the olfactory route is largely distributed in astroglia (Henriksson et al., 1999). Moreover, a link between glutamine synthetase and Ca^{2+} influx has been postulated for astroglia (Benjamin, 1987; Pearce et al., 1986). Therefore, it is hypothesized that reactive astroglia can accelerate Mn uptake and accumulation due to the hyperactivity or high density of glial cells. The purpose of this study

was to investigate whether MEMRI can enhance reactive astroglia (astrogliosis) after focal ischemia *in vivo*. Mn-enhanced T₁-, T₂- and diffusion-weighted MR images were acquired 1 day (acute phase), 11 days (inflammation phase), and 22 days (chronic phase) after transient middle cerebral artery occlusion (MCAO) in the rat. In addition, hematoxylin–eosin (HE) staining and immunohistochemical stainings such as GFAP (glial fibrillary acidic protein), Iba1 (ionized calcium binding adaptor molecule-1) (Schluesener et al., 1998), TUNEL (TdT-mediated dUTP-biotin nick end labeling), and ssDNA (single-stranded DNA) (Frankfurt et al., 1996) were performed, and the results were compared to MRIs after image registration. Preliminary versions of this work have been presented previously (Kawai et al., 2005).

Materials and methods

Animal experiments

All animal experiments were approved by the Meiji University of Integrative Medicine Institutional Animal Care and Use Committee (Kyoto, Japan).

Experimental procedure

Twenty-four male Sprague-Dawley rats (284.0±33.2 g, *n*=24, Shimizu Experimental Animal, Inc., Japan) were divided into six groups as 1 day after MCAO (*n*=5), 11 days after MCAO (*n*=5), 22 days after MCAO (*n*=5), 1 day after a sham operation (*n*=3), 11 days after sham (*n*=3), and 22 days after sham (*n*=3). For the three MCAO groups, the middle cerebral artery (MCA) was occluded for 60 minutes, while for the sham groups, the same operation was performed but without occlusion. During the MCAO or sham operations, diffusion-weighted MRI and MR angiography were acquired as a preliminary measurement to check the occlusion of the MCA, bleeding, and edematous changes in the brain. After reperfusion, 50 mM of MnCl₂ solution (MnCl₂·4H₂O; Sigma, St. Louis, MO) was administered immediately for day 1 MCAO and sham groups, 10 days later for day 11 MCAO and sham groups, and 21 days later for day 22 MCAO and sham groups (Fig. 1a). MRI data were acquired exactly 24 hours after MnCl₂ administration for all groups. Finally, perfusion fixation was performed and the brain was extracted for immunohistochemical staining.

Animal preparation for the transient MCAO model

The rats were initially anesthetized with 4.0% isoflurane (Abbott Japan, Japan) for intubation, and then maintained with 2.0–2.5% isoflurane mixed with a 1:5 O₂/room air gas mixture using a rodent ventilator (SAR-830/AP, CWE, Inc., PA). Rectal temperature was continuously monitored and automatically maintained at approximately 37.5 °C using a temperature controller (E5GN, Omron, Inc., Japan) and electrical heating pad (SG-15, Showa-Seiki industry, Inc., Japan). Polyethylene tube (PE-50, Becton, Dickinson and Company, NJ) was placed in the femoral artery and arterial blood was sampled to measure carbon dioxide partial pressure (pCO₂), oxygen partial pressure (pO₂), and pH (i-STAT, Abbott Laboratories, NJ) immediately before the MCAO or sham operations. In addition, the end-tidal CO₂ and anesthetic gas concentration were monitored using a gas analyzer (CX-2, Korin, Japan). For the three MCAO model groups, the MCA was temporarily occluded for 60 minutes based on the method of Longa et al. (1989). The tips of the nylon sutures (GA04NA, Alfresa Pharma Inc., Japan) were coated with a silicone rubber impression

material mixed with hardening agent (Xantopren-L and Optosil, Heraeus Kulzer Co., Dormagen, Germany). The tip diameter was within 0.40 ± 0.05 mm as assessed using a stereoscopic microscope (TS100, Nikon, Japan). The MCA was occluded by inserting the nylon suture into the internal carotid artery via the external carotid artery, after which the blood flow in the MCA, brain edema, and intracerebral bleeding were checked by a MRI scan (preliminary MRI measurements). Sixty minutes after the occlusion, the sutures were carefully removed from the MCA for reperfusion. MnCl_2 solution was then immediately administered for the Day 1 group, otherwise the animal was moved to a cage after suturing. The same procedures were performed for the three sham groups, but without insertion of the suture.

Manganese-enhanced MRI

MnCl_2 administration was performed exactly 24 hours before MRI measurements for all groups as described in a previous report (Aoki et al., 2004; Silva et al., 2004). Prior to the administration, 100 mM of MnCl_2 ($\text{MnCl}_2 \cdot 4\text{H}_2\text{O}$, Sigma, St. Louis, MO) was dissolved in distilled water and diluted to 50 mM by saline in order to match the osmotic pressure to that of blood. We slowly infused the 50 mM osmotic pressure-controlled MnCl_2 solution ($378.9 \mu\text{mol/kg}$) at a rate of 2.0 ml/hour through the tail vein using a syringe pump (KDS-100, KD Scientific, Inc. MA). During MnCl_2 infusion, anesthesia was maintained with a concentration of 0.5–1.0% isoflurane. After administration, saline (6.7 ml/100 g) was subcutaneously injected into the back skin, after which the animals were placed in an incubator (30–32 °C, E5GN and SG-15) for 12 hours to maintain body temperature. We performed all MEMRI procedures following the guidelines of the Animal Care and Use Committee and the Animal Health & Care Section of the National Institute of Neurological Disorders and Stroke, National Institutes of Health (Bethesda, MD).

MRI measurements

Proton MRI measurements were performed in a 4.7-T horizontal magnet (General electric, NY) with a 90-mm-diameter gradient coil (Resonance Research Inc., MA) interfaced to a Bruker Avance console (Bruker Biospin GmbH, Germany). Animals were anesthetized using the same procedure as described for the MCAO model (see above), and during the measurements, rectal temperature was maintained at approximately 37.5 °C using a temperature control unit (Rapid Biomedical GmbH). A 69-mm inner diameter birdcage and quadrature-polarized surface RF coils were used for transmitting and receiving, respectively (Rapid Biomedical GmbH). T_1 , T_2 , and diffusion-weighted two-dimensional (2D) multislice spin-echo MR images were obtained. Two T_1 -weighted MRIs were acquired with the following parameters: repetition time (TR)/echo time (TE)=170/9 ms, matrix size=256×256, field of view (FOV)=32×32 mm², slice thickness (ST)=1.2 mm, slice gap=0.8 mm, and number of averages (NA)=8. Coronal (6 slices with and without a 1-mm slice offset) and horizontal (5 slices with and without a 1 mm slice offset) slice orientations were selected with a $125 \times 125 \times 1200\text{-}\mu\text{m}^3$ nominal voxel resolution. T_2 and diffusion-weighted MRIs were also acquired with the following parameters: TR/TE=3000/80 ms, matrix size=256×192, FOV=32×32 mm², ST=1.2 mm, slice gap=0.8 mm, and NA=8. The diffusion gradients were applied in the *z*-direction with the following parameters: diffusion sensitivity (*b*-value)=47 s/mm² (minimum value of the system) for the T_2 -weighted image

and 1500 s/mm^2 for the diffusion-weighted MRI, gradient strength (G)=0 and 92.3 mT/m , gradient duration (δ)=10 ms, and interval between the gradient pulse onset (Δ)=27 ms. A coronal (6 slices without slice offset) slice orientation was selected with a $125 \times 167 \times 1200\text{-}\mu\text{m}^3$ nominal voxel resolution.

Preliminary MRI experiment during MCA occlusion

A quick MRI observation was performed during the occlusion to check the condition of the MCA and brain edema. Diffusion-weighted MRI was acquired to check brain edema after ischemia (spin-echo, TR/TE=2500/80 ms, matrix size=256×128, FOV=32×32 mm², ST=1.2 mm, slice gap=0.8 mm, NA=1, slice orientation=coronal, and scan time=6 min), and MR angiography was performed to check occlusion of the MCA (3D gradient-echo, TR/TE=9/5.8 ms, matrix size= 128×128×16, FOV=32×32×9.8 mm³, NA=2, and scan time=60 s).

Immunohistochemical staining and histopathological examination

Perfusion fixation was performed immediately after the MRI acquisition using a saline and 10% formalin solution (Wako, Japan), after which the brain was carefully extracted. The extracted brain was embedded using paraffin after alcoholic dehydration. Seven slices (1.5, 1.0, 0.5, 0.0, -0.5, -1.0, and -1.5 mm from the bregma) were stained with HE and four slices (1.5, 0.5, -0.5, and -1.5 mm from the bregma) were stained with TUNEL, ssDNA, Iba1, and GFAP. Digital microphotographs were taken of every preparation in a region of interest (ROI) similar to that of the MRI using the following tools: microscope Eclipse E800 (Nikon, Japan), digital camera DXM1200 (Nikon), 4× or 40× lens (Nikon), and ACT-1 imaging software (Nikon). The digital images were processed for the GFAP and Iba1 stainings to automatically determine the positive-stained area as follows: (1) the brightness and contrast were automatically optimized (Photoshop™, Ver. 8.0.1, Adobe, Inc., CA); (2) the blue-stained intact cell nuclei were removed using the “color replacement tool” (allowance value=200; Photoshop); (3) the brown-stained positive cells were enhanced using the “color replacement tool” (allowance value=100; Photoshop); (4) the color image was converted to a black-and-white binary map using a 50% threshold, (5) the size of the positive cell area (black area) was determined (ImageJ, NIH, MD). The ratio of the positive cell area-to-total area was then calculated. For the TUNEL or ssDNA stainings, an outside observer counted the number of brown-stained positive cells and blue-stained negative cells inside a $0.25 \times 0.3 \text{ mm}^2$ matrix in each ROI (non-affected CPU, ischemic periphery, and ischemic core) using a double-blind method. The ratio of positive cells was then calculated as:

$$\text{Ratio of no. positive cells} = \frac{\text{no. positive cells}}{(\text{no. negative cells} + \text{no. positive cells})}.$$

Data and statistical analysis

Quantitative apparent diffusion coefficient maps were calculated from a linear least-squares fitting to the T_2 -weighted (b -value= 47 s/mm²) and diffusion-weighted (b -value=1500 s/mm²) MRI using the MRVision image analysis software (Version 1.6.4, MRVision Co., MA) on a Linux PC (xw4100, Hewlett-Packard Japan, Japan). For comparison of signal intensities, ROIs were defined as follows: (1) the signal intensities and standard deviation

(SD) were calculated on the contralateral side of the CPU with reference to Paxinos's brain map; (2) a contour was drawn around the enhanced area defined using a threshold of $2 \times \text{SD}$ of the contralateral CPU; (3) three landmark points were manually set on the contour and an ellipse was fitted to the landmarks; (4) the ischemic core was determined as the small ellipse having major and minor axes half the length of the fitted ellipse (Fig. 1b, red region); and (5) the ischemic periphery was determined as the region remaining after removing the ischemic core from the fitted ellipse (Fig. 1b, blue region). For the sham groups, we used the same ROIs for both the ischemic core and periphery in the CPU. The MR signal intensities were compared (Prism, Ver. 4, GraphPad Software, CA, USA) using Tukey's multiple comparison test, the immunohistochemical stainings with one-way ANOVA with Tukey's correction, the blood gas analysis using an unpaired *T* test, and the body temperature measurements using Tukey's multiple comparison test. The statistical significance was set to $P < 0.05$ for each analysis, and all data are presented as mean \pm SD.

Results

Generation of transient MCAO model

We generated transient MCAO and sham operation models. Initial assessment with MR angiography demonstrated that MCA blood flow was occluded for every MCAO model (data not shown). It was also confirmed that arterial blood gas readings were within normal physiological ranges prior to both the MCAO and sham operations. No significant statistical difference in these parameters was observed between the MCAO and sham-operated groups (Table 1). We observed that body temperature was well maintained before and after MCAO for every group using an automatic heating system (Table 1). For the sham group, no signal asymmetry in the brain was observed on either the MEMRI (T_1 -weighted MRI), T_2 -, or diffusion-weighted MRI (Figs. 1c–e).

MEMRI detection of ring-shaped signal enhancement after MCAO

Ring- or crescent-shaped signal enhancement (Figs. 2b', c', yellow arrows) was found in the peripheral region of the ischemic core for day 11 and day 22 after MCAO groups. In contrast, no ischemia-related signal changes were observed for any of the sham groups (Fig. 1c), although the signal intensity was increased throughout the entire brain similar to the results of previous reports (Aoki et al., 2004). In rats at 1 day after MCAO, significant signal reduction was observed on the affected side of the caudate putamen (CPU) (Figs. 2a, a', and d). On the other hand, no signal reduction was observed in the contralateral and unaffected brain tissues (Figs. 2a, a', and d). At 11 days after MCAO, a ring- or crescent-shaped Mn-related enhancement was clearly observed surrounding the ischemic core (Figs. 2b, b', and e). A similar enhancement was also seen at 22 days after MCAO although the contralateral and unaffected tissues lost Mn-related enhancement (Figs. 2c, c', and e). The highest signal intensity was observed in an area between the lateral ventricle and ischemic region (Figs. 2b' and c', red arrows). Thus, ring- or crescent-shaped enhancement in MEMRI was observed in the ischemic periphery at both 11 and 22 days after MCAO.

Changes in T₂- and diffusion-weighted MR images after MCAO

Significant signal enhancements were observed in the ipsilateral CPU 1 day after MCAO for both T₂- and diffusion-weighted MRI (Figs. 3a, b, g, and h), in agreement with the region exhibiting signal reduction in the MEMRI (Fig. 2a). At 11 days after MCAO, tachetic and feeble signal enhancement was observed on the lateral side of the CPU in the T₂-weighted MRI (Fig. 3c). On the other hand, no signal enhancement was observed in the diffusion-weighted MRI (Figs. 3d and g). T₂ and diffusion signal reduction was found in the area corresponding to the ring-shaped signal enhancement in the MEMRI at 11 days (Figs. 3c and d). At 22 days after MCAO, a slight signal reduction in the CPU was observed on the T₂- and diffusion-weighted MR images (Figs. 3e, f, and h).

Comparison between MEMRI and histochemical and immunohistochemical stainings

We discovered that ring- or crescent-shaped enhancement in the MEMRI agreed well with the GFAP-positive region reflecting reactive astroglia at both 11 and 22 days after MCAO (Figs. 4a and b). The highest density of GFAP-positive cells was observed in the area between the lateral ventricle and ischemic region, and this agreed with the localization of signal enhancement in MEMRI (Figs. 4a, b, red arrows, Fig. 5a). On the other hand, signal enhancement in MEMRI did not spatially agree with the distribution of the Iba1 immunoreactivity (Figs. 4a and c) or necrotic core identified by HE staining (Figs. 4a and d), although the distribution of the Iba1-positive cells did partially overlap the MEMRI enhancement because the Iba1-positive cells were observed throughout the entire ischemic region (Figs. 4c and b). The distribution of Iba1-positive cells at 11 and 22 days after MCAO corresponded to the necrotic region shown in the HE staining and T₂-weighted MRI (Figs. 4c–e, blue).

No unilateral increment of GFAP- or Iba1-positive cells was found at 1 day after MCAO (Figs. 5a and b and 6a-1, a'-1, and b-1). The HE staining indicated that there was a slight decrease in cell density in the affected CPU at this time point (Fig. 6c-1), corresponding to signal enhancement in T₂- and diffusion-weighted MRI (Figs. 3a and b). At 11 days after MCAO, we clearly observed GFAP-positive cells in the periphery of the ischemic region (Figs. 4b, 5a, and 6a-2 and a'-2), although Iba1-positive cells were distributed throughout the ischemic core (Figs. 5b and 6b-2). In comparison with the day 11 group, a similar distribution of proliferated GFAP-positive cells was presented at 22 days after MCAO (Figs. 5a and 6a-3 and a'-3), although the number of Iba1-positive cells in the ischemic core decreased (Figs. 5b and 6b-3).

We also evaluated DNA fragmentation using TUNEL and ssDNA immunohistochemical stainings to determine whether apoptotic cells contribute to the MEMRI signal enhancement (Figs. 5c and d and 7). TUNEL- or ssDNA-positive cells were present in a small percentage (2.8%) of the peripheral ischemic region in the 22 days after MCAO group (Fig. 5c), while most of the tissue (43.1%) was replaced by reactive astroglia (Figs. 5a and 7a). In addition, the density of TUNEL- or ssDNA-positive cells was high in the ischemic core at the day 1 stage and in the periphery at the day 11 stage (Figs. 5c and d). Thereafter, the number of apoptotic cells in the ischemic region decreased significantly for the day 22 phase (Figs. 5c

and d), although the higher accumulation of Mn in the ring-shaped region was still observed at this time (Figs. 2c and d and c').

Discussion

We demonstrated that MEMRI can detect proliferated reactive gliosis after MCAO in the rat brain. As controlling reactive astroglia is an important key to successful treatment after CNS insults, our data support the potential utility of MEMRI in monitoring the progression and therapeutic suppression of neuropathologies. For the development of drugs capable of regulating reactive gliosis and the optimization of administration protocols for treatments, an *in vivo* visualization method that can be used to precisely longitudinally assess astroglia is necessary. Although MEMRI cannot be used directly for humans in the clinical field because of the toxicity of Mn (Sloot and Gramsbergen, 1994), it will aid in accelerating basic research towards gaining insights into the mechanisms of neural regeneration and suppressing inflammation after CNS disturbance.

Pathological correlates of signal enhancements in MEMRI

There are at least five possible sources for the enhanced signal found in the MEMRI: (1) dense accumulation of reactive astroglia; (2) necrotic $\text{Ca}^{2+}/\text{Mn}^{2+}$ influx; (3) migration of microglia; (4) disruption of blood–brain barrier (BBB) and migration of inflammatory blood cells; and (5) apoptosis. The contribution of each of these possibilities is assessable based on the present observations as follows:

1. To investigate the mechanism of the signal enhancement, we designed and compared three different phases consisting of 1 day after transient MCAO as an acute phase model, 11 days as an inflammation phase model, and 22 days as a chronic phase model. Ring- or crescent-shaped regional signal enhancement in MEMRI was observed at both 11 days and 22 days (Figs. 2b and c), and localization of this change was in good agreement with that of the GFAP-positive stained cells (Figs. 4a, b and 5a). In addition, the ischemic periphery, especially near the lateral ventricles, was dominated by GFAP-positive astrocytes (Figs. 5a and 7a). This formation of GFAP-positive cells agreed well with many previous reports describing reactive astroglia (Clark et al., 1993; Garcia et al., 1993; Schmidt-Kastner et al., 1990). The increase in GFAP-positive cells peaked around 48 hours after ischemia and was maintained for 5 weeks (Petito et al., 1990). In contrast, the distributions of the other stainings (such as HE, Iba1, TUNEL, and ssDNA) did not agree with the location of the enhanced MEMRI signals. These results suggest that reactive gliosis due to the proliferation of astroglia is the dominant mechanism causing the ring- or crescent-shaped signal enhancement in MEMRI.
2. A rapid Ca^{2+} influx into the cells after ischemia induces necrosis. The Ca^{2+} influx related to cell death can potentially enhance the signal intensity in MEMRI (DeGraba et al., 1993). In a BBB-disrupted animal model, Mn^{2+} accumulates in the neuron/glia immediately after somatosensory stimulation (Lin and Koretsky, 1997), insults such as anoxic depolarization induced by MCAO

(Aoki et al., 2003), and spreading depression induced by potassium chloride exposure (Henning et al., 2005). There are differences in the experimental conditions between the intact and disrupted BBB models because Mn^{2+} in the plasma can directly reach the extracellular fluid of neurons and glia in the case of BBB-disrupted models (Aoki et al., 2003; Lin and Koretsky, 1997). Thus, using MEMRI with a BBB-disrupted model reflects the Ca^{2+} influx from extracellular fluid through Ca^{2+} channels. On the other hand, in a normal brain, most of the Mn^{2+} is blocked by the BBB immediately after systemic administration (Aoki et al., 2004; Lin and Koretsky, 1997). In our 'intact BBB model', signal enhancement in the T_1 -weighted MRI was not observed in the ischemic core at the day 1 phase (Figs. 2a and a') despite the fact that the ischemic core has longer T_2 (Fig. 3a). This suggests that Mn concentration in the ischemic core was low at the day 1 phase in comparison with normal tissue. We hypothesize that Mn transportation from ependymal cells into the CNS was hindered due to low blood supply, edematous changes, and/or Ca^{2+} channel disturbance by ischemic cytotoxicity. If MEMRI predominantly reflects anoxic depolarization in the acute phase for this ischemic model, signal in the ischemic core must be enhanced because enhanced signal remains for longer than 1 day (Aoki et al., 2004). Therefore, we conclude that anoxic depolarization is not a dominant contributor to the MEMRI signal enhancement in our intact BBB model.

3. The migration of microglia, namely reactive microglia (microgliosis), was observed across the entire ischemic region at the day 11 'inflammation phase' (Fig. 6b-2). Reactive microglia were activated 3 hours after reperfusion and showed phagocytic activity in dead pyramidal cells 7 days later (Korematsu et al., 1994). Microglia are activated in connection with astrogliosis (Perry and Andersson, 1992) and release glutamate (Piani et al., 1992). Thus, microglia have been proposed as a causative factor for Mn enhancement in MRI (Wideroe et al., 2009). However, the migrated microglia were distributed throughout the necrotic region of the ischemic core so that the localization did not correspond to the ring- or crescent-shaped region observed in both the day 11 and day 22 MEMRI (Fig. 4a vs. 4c, Fig. 2c vs. Fig. 6b-3). This was also supported by the observation that the Iba1-positive cells appeared only for the day 11 inflammation phase (Figs. 5b and 6b), while MEMRI signal did not dramatically change between 11 and 22 days (Figs. 2b, c, and e). On the other hand, GFAP-positive astroglia formed a high cell-density barrier surrounding the inflamed ischemic core (Figs. 4b and 7a), and this led to high signal intensity in the MEMRI (Fig. 4a). Although microglia migration may also partially contribute to the enhanced MEMRI signal intensity, it is not a dominant cause of the ring- or crescent-shaped enhancement observed in this ischemic model because of the homogeneous distribution and low cell volume density.
4. Mn can enter the CNS through a BBB-disrupted area. Clinically, Gd-DTPA can be used to detect brain tumor with MRI because of the incomplete BBB formation (Runge et al., 1985). In our results, there was no MEMRI enhancement in the ischemic core throughout the entire experimental period

(Figs. 2f and 4a, d, and e). If we assume that enhancement of MEMRI is caused by disruption of the BBB, the ischemic core must be enhanced because disrupted BBB can easily infiltrate the Mn^{2+} into the CNS. We speculate that: (a) the cell density was low due to decidualization; (b) Mn did not accumulate in the cells due to functional disorder of Ca^{2+} channels; and (c) Mn was washed out of the ischemic core rapidly because the MEMRIs were acquired 24 hours after Mn administration and the half-life of Mn in blood is short (Gerdin et al., 1985). Therefore, it is reasonable to conclude that BBB disruption is not a dominant contributor to MEMRI enhancement. On the other hand, BBB disruption allows the migration of not only microglia but also peripheral inflammatory cells such as monocytes, macrophages, T lymphocytes, natural killer cells, and polymorphonuclear neutrophil leukocytes (Garcia and Kamijyo, 1974). Migration of these inflammatory cells is also a potential contributor to MEMRI enhancement. However, disagreement between the necrotic and MEMRI enhanced areas (Figs. 4d and e) similarly suggests that signal enhancement did not originate from migration of inflammatory cells in the ischemic model.

5. Another candidate for signal enhancement in the MEMRI is apoptosis. Slight and prolonged Ca^{2+} influx into cells injures mitochondria (Martin et al., 1998) and activates caspase cascade (Siesjo et al., 1999). Apoptosis is also an important factor in balancing cell proliferation and elimination (Lang et al., 2005) and is known to be triggered by high cell density. Therefore, apoptosis has the potential to enhance MEMRI signal not only through an ischemic energy deficit but also by proliferating glial cells. In our study, TUNEL- or ssDNA-positive cells were predominantly observed in the ischemic core at the day 1 stage (Figs. 5c and d), although MEMRI was not enhanced at that time point (Fig. 2a). Thereafter, the number of apoptotic cells in the ischemic region significantly decreased at the day 22 stage (Figs. 5c and d), although this change did not agree with the enhancement of the MEMRI (Fig. 2c). In addition, the occupancy of apoptotic cells was not high ($2.8 \pm 1.9\%$ for TUNEL, $1.1 \pm 1.1\%$ for ssDNA) in comparison with the astroglia ($43.1 \pm 10.8\%$ at GFAP) found in the day 22 phase. Therefore, it is reasoned that apoptosis is also not a dominant factor contributing to MEMRI signal enhancement.

Therefore, the present evidence strongly suggests that the dominant mechanism for ring- or crescent-shaped enhancement in MEMRI is the reactive astroglia after stroke rather than BBB disruption, necrosis, or apoptotic degeneration. In addition, hyper-active microglia and migrated reactive microglia (microgliosis) may partially contribute to the enhancement. Although the contribution of mossy fiber sprouting was reported for an epilepsy model in the rat hippocampus (Immonen et al., 2008; Nairismagi et al., 2006), the mossy fibers exist only in the hippocampal CA3 and dentate gyrus (DG) and therefore discussion of this factor has been excluded.

MEMRI contrast mechanism

The mechanism behind MEMRI signal enhancement has been previously discussed in relation to experimental models of hypoxia (Wideroe et al., 2009; Yang and Wu, 2008),

kainic acid-induced hippocampal injury (Immonen et al., 2008; Nairismagi et al., 2006), cathepsin D deficiency (Haapanen et al., 2007), and transient brain ischemia (Kawai et al., 2005). Ischemic or lesion models always involve multiple factors such as gliosis (Kawai et al., 2005), necrosis, mossy fiber spouting in the hippocampus (Immonen et al., 2008; Nairismagi et al., 2006), microglia migration (Haapanen et al., 2007; Wideroe et al., 2009), and Mn-SOD and GS enzymatic activities (Yang and Wu, 2008). To clarify these issues, we designed our protocol to consist of three different phases after stroke and five different immunostainings so as to discriminate among microglia/astroglia proliferations, necrotic/apoptotic alterations, and inflammatory responses.

We propose that two physical/physiological factors predominantly contribute to MEMRI contrast in the ischemic brain. First, the Ca^{2+} channel activity and $\text{Mn}^{2+}/\text{Ca}^{2+}$ influx in the cells is a possible factor. The most likely cause of MEMRI enhancement is Mn accumulation through voltage-gated Ca^{2+} channels (Hunter et al., 1980; Narita et al., 1990). Mn accumulation in the activated brain region is triggered by somatosensory stimulation and glutamate administration in a BBB disrupted rat model (Lin and Koretsky, 1997) and can be suppressed by a Ca^{2+} channel blocker such as verapamil (Narita et al., 1990). In addition, it has been reported that interaction exists between glutamate receptors and Ca^{2+} channel openings (Pearce et al., 1986) and that there is a link between glutamine synthetase and Ca^{2+} in astroglia (Benjamin, 1987). Therefore, the Ca^{2+} channel activity of astroglia is an important factor in MEMRI signal enhancement. Note that Mn-superoxide dismutase (Mn-SOD) and glutamine synthetase may also participate in the process (Yang and Wu, 2008).

Secondly, increments in the cell density can also contribute to MEMRI signal enhancement. In our experiments, excessive increase of the cell density due to hyper proliferation of astroglia was observed (Figs. 5a and 7a) and corresponded to the ring- or crescent-shaped MEMRI enhancement (Figs. 4a and b). Thus, it is speculated that the hyperactivity of Ca^{2+} channels in the cells and/or replacement of normal tissue by proliferated reactive astroglia are the predominant mechanisms driving signal enhancement in the MEMRI after brain ischemia.

Conclusion

This study demonstrated good agreement between MEMRI signal enhancement and gliosis, predominantly GFAP-positive astroglia, reacting to transient MCAO. In contrast, the presence of apoptotic cells (as evaluated by TUNEL and ssDNA), and the size of the necrotic region (as evaluated by HE staining) did not agree with the area showing MEMRI signal enhancement. We suggest that high cell density and/or hyperactivity corresponding to reactive astroglia was the dominant factor behind the MEMRI enhancement after brain ischemia. In addition, increased Mn accumulation in hyperactive microglia and the migration of reactive microglia (microgliosis), may also partially contribute to the enhancement. The MEMRI technique will provide useful information for the evaluation of stem cell transplantation, drug development for neural regeneration, and anti-inflammation *in vivo*.

Acknowledgments

The authors thank Ms. Noriko Matsumoto (Meiji University of Integrative Medicine) for generating the animal models, Dr. Alan P Koretsky (Chief, Laboratory of Functional and Molecular Imaging, NINDS, NIH), and Dr. Iwao Kanno (Director, Molecular Imaging Center, National Institutes of Radiological Science) for excellent discussion and editing. This work was partly supported by Grants-in-Aid for Scientific Research (Kakenhi) of the Japan Society for the Promotion of Science (JSPS).

References

- Aoki I, Ebisu T, Tanaka C, Katsuta K, Fujikawa A, Umeda M, Fukunaga M, Takegami T, Shapiro EM, Naruse S. Detection of the anoxic depolarization of focal ischemia using manganese-enhanced MRI. *Magn Reson Med*. 2003; 50:7–12. [PubMed: 12815672]
- Aoki I, Wu YJ, Silva AC, Lynch RM, Koretsky AP. *In vivo* detection of neuroarchitecture in the rodent brain using manganese-enhanced MRI. *NeuroImage*. 2004; 22:1046–1059. [PubMed: 15219577]
- Benjamin AM. Influence of Na⁺, K⁺, and Ca²⁺ on glutamine synthesis and distribution in rat brain cortex slices: a possible linkage of glutamine synthetase with cerebral transport processes and energetics in the astrocytes. *J Neurochem*. 1987; 48:1157–1164. [PubMed: 2434618]
- Bush TG, Puvanachandra N, Horner CH, Polito A, Ostefeld T, Svendsen CN, Mucke L, Johnson MH, Sofroniew MV. Leukocyte infiltration, neuronal degeneration, and neurite outgrowth after ablation of scar-forming, reactive astrocytes in adult transgenic mice. *Neuron*. 1999; 23:297–308. [PubMed: 10399936]
- Carl GF, Blackwell LK, Barnett FC, Thompson LA, Rissinger CJ, Olin KL, Critchfield JW, Keen CL, Gallagher BB. Manganese and epilepsy: brain glutamine synthetase and liver arginase activities in genetically epilepsy prone and chronically seized rats. *Epilepsia*. 1993; 34:441–446. [PubMed: 8099325]
- Clark RK, Lee EV, Fish CJ, White RF, Price WJ, Jonak ZL, Feuerstein GZ, Barone FC. Development of tissue damage, inflammation and resolution following stroke: an immunohistochemical and quantitative planimetric study. *Brain Res Bull*. 1993; 31:565–572. [PubMed: 8495380]
- DeGraba TJ, Ostrow PT, Grotta JC. Threshold of calcium disturbances after focal cerebral ischemia in rats. Implications of the window of therapeutic opportunity. *Stroke*. 1993; 24:1212–1216. discussion 1216–1217. [PubMed: 7688156]
- Faulkner JR, Herrmann JE, Woo MJ, Tansey KE, Doan NB, Sofroniew MV. Reactive astrocytes protect tissue and preserve function after spinal cord injury. *J Neurosci*. 2004; 24:2143–2155. [PubMed: 14999065]
- Frankfurt OS, Robb JA, Sugarbaker EV, Villa L. Monoclonal antibody to single-stranded DNA is a specific and sensitive cellular marker of apoptosis. *Exp Cell Res*. 1996; 226:387–397. [PubMed: 8806443]
- Garcia JH, Kamijyo Y. Cerebral infarction. Evolution of histopathological changes after occlusion of a middle cerebral artery in primates. *J Neuropathol Exp Neurol*. 1974; 33:408–421. [PubMed: 4209682]
- Garcia JH, Yoshida Y, Chen H, Li Y, Zhang ZG, Lian J, Chen S, Chopp M. Progression from ischemic injury to infarct following middle cerebral artery occlusion in the rat. *Am J Pathol*. 1993; 142:623–635. [PubMed: 8434652]
- Gerdin B, McCann E, Lundberg C, Arfors KE. Selective tissue accumulation of manganese and its effect on regional blood flow and haemodynamics after intravenous infusion of its chloride salt in the rat. *Int J Tissue React*. 1985; 7:373–380. [PubMed: 4055262]
- Giulian D. Reactive glia as rivals in regulating neuronal survival. *Glia*. 1993; 7:102–110. [PubMed: 8423057]
- Goldshmit Y, Galea MP, Wise G, Bartlett PF, Turnley AM. Axonal regeneration and lack of astrocytic gliosis in EphA4-deficient mice. *J Neurosci*. 2004; 24:10064–10073. [PubMed: 15537875]
- Haapanen A, Ramadan UA, Autti T, Joensuu R, Tyynela J. *In vivo* MRI reveals the dynamics of pathological changes in the brains of cathepsin D-deficient mice and correlates changes in manganese-enhanced MRI with microglial activation. *Magn Reson Imaging*. 2007; 25:1024–1031. [PubMed: 17451907]

- Henning EC, Meng X, Fisher M, Sotak CH. Visualization of cortical spreading depression using manganese-enhanced magnetic resonance imaging. *Magn Reson Med*. 2005; 53:851–857. [PubMed: 15799040]
- Henriksson J, Tallkvist J, Tjalve H. Transport of manganese via the olfactory pathway in rats: dosage dependency of the uptake and subcellular distribution of the metal in the olfactory epithelium and the brain. *Toxicol Appl Pharmacol*. 1999; 156:119–128. [PubMed: 10198277]
- Hunter DR, Komai H, Haworth RA, Jackson MD, Berkoff HA. Comparison of Ca^{2+} , Sr^{2+} , and Mn^{2+} fluxes in mitochondria of the perfused rat heart. *Circ Res*. 1980; 47:721–727. [PubMed: 6774832]
- Immonen RJ, Kharatishvili I, Sierra A, Einula C, Pitkanen A, Grohn OH. Manganese enhanced MRI detects mossy fiber sprouting rather than neurodegeneration, gliosis or seizure-activity in the epileptic rat hippocampus. *NeuroImage*. 2008; 40:1718–1730. [PubMed: 18328732]
- John GR, Lee SC, Brosnan CF. Cytokines: powerful regulators of glial cell activation. *Neuroscientist*. 2003; 9:10–22. [PubMed: 12580336]
- Kawai, Y., Aoki, I., Matsumoto, N., Umeda, M., Higuchi, T., Silva, AC., Koretsky, AP., Tanaka, T. Detection of neural dysfunction for focal ischemia using manganese-enhanced MRI (MEMRI) in the rat brain. The Fourth Annual Meeting of the Society for Molecular Imaging (SMI); Cologne, Germany. 2005. p. 397
- Korematsu K, Goto S, Nagahiro S, Ushio Y. Microglial response to transient focal cerebral ischemia: an immunocytochemical study on the rat cerebral cortex using anti-phosphotyrosine antibody. *J Cereb Blood Flow Metab*. 1994; 14:825–830. [PubMed: 7520452]
- Lang F, Foller M, Lang KS, Lang PA, Ritter M, Gulbins E, Vereninov A, Huber SM. Ion channels in cell proliferation and apoptotic cell death. *J Membr Biol*. 2005; 205:147–157. [PubMed: 16362503]
- Lin YJ, Koretsky AP. Manganese ion enhances T_1 -weighted MRI during brain activation: an approach to direct imaging of brain function. *Magn Reson Med*. 1997; 38:378–388. [PubMed: 9339438]
- Longa EZ, Weinstein PR, Carlson S, Cummins R. Reversible middle cerebral artery occlusion without craniectomy in rats. *Stroke*. 1989; 20:84–91. [PubMed: 2643202]
- Martin LJ, Al-Abdulla NA, Brambrink AM, Kirsch JR, Sieber FE, Portera-Cailliau C. Neurodegeneration in excitotoxicity, global cerebral ischemia, and target deprivation: a perspective on the contributions of apoptosis and necrosis. *Brain Res Bull*. 1998; 46:281–309. [PubMed: 9671259]
- Mendonca DM, Gaggelli E, Lauterbur PC. Paramagnetic contrast agents in nuclear magnetic resonance medical imaging. *Semin Nucl Med*. 1983; 13:364–376. [PubMed: 6359418]
- Menet V, Prieto M, Privat A, Gimenez y Ribotta M. Axonal plasticity and functional recovery after spinal cord injury in mice deficient in both glial fibrillary acidic protein and vimentin genes. *Proc Natl Acad Sci U S A*. 2003; 100:8999–9004. [PubMed: 12861073]
- Nairismagi J, Pitkanen A, Narkilahti S, Huttunen J, Kauppinen RA, Grohn OH. Manganese-enhanced magnetic resonance imaging of mossy fiber plasticity *in vivo*. *NeuroImage*. 2006; 30:130–135. [PubMed: 16246593]
- Narita K, Kawasaki F, Kita H. Mn and Mg influxes through Ca channels of motor nerve terminals are prevented by verapamil in frogs. *Brain Res*. 1990; 510:289–295. [PubMed: 2158851]
- Norenberg MD. Astrocyte responses to CNS injury. *J Neuropathol Exp Neurol*. 1994; 53:213–220. [PubMed: 8176405]
- Norenberg MD, Martinez-Hernandez A. Fine structural localization of glutamine synthetase in astrocytes of rat brain. *Brain Res*. 1979; 161:303–310. [PubMed: 31966]
- Okada S, Nakamura M, Katoh H, Miyao T, Shimazaki T, Ishii K, Yamane J, Yoshimura A, Iwamoto Y, Toyama Y, Okano H. Conditional ablation of Stat3 or Socs3 discloses a dual role for reactive astrocytes after spinal cord injury. *Nat Med*. 2006; 12:829–834. [PubMed: 16783372]
- Pearce B, Albrecht J, Morrow C, Murphy S. Astrocyte glutamate receptor activation promotes inositol phospholipid turnover and calcium flux. *Neurosci Lett*. 1986; 72:335–340. [PubMed: 3029635]
- Perry VH, Andersson PB. The inflammatory response in the CNS. *Neuropathol Appl Neurobiol*. 1992; 18:454–459. [PubMed: 1454134]
- Petito CK, Morgello S, Felix JC, Lesser ML. The two patterns of reactive astrocytosis in postischemic rat brain. *J Cereb Blood Flow Metab*. 1990; 10:850–859. [PubMed: 2211878]

- Piani D, Spranger M, Frei K, Schaffner A, Fontana A. Macrophage-induced cytotoxicity of *N*-methyl-D-aspartate receptor positive neurons involves excitatory amino acids rather than reactive oxygen intermediates and cytokines. *Eur J Immunol.* 1992; 22:2429–2436. [PubMed: 1355433]
- Runge VM, Clanton JA, Price AC, Wehr CJ, Herzer WA, Partain CL, James AE Jr. The use of Gd DTPA as a perfusion agent and marker of blood–brain barrier disruption. *Magn Reson Imaging.* 1985; 3:43–55. [PubMed: 3923292]
- Schluesener HJ, Seid K, Kretzschmar J, Meyermann R. Allograft-inflammatory factor-1 in rat experimental autoimmune encephalomyelitis, neuritis, and uveitis: expression by activated macrophages and microglial cells. *Glia.* 1998; 24:244–251. [PubMed: 9728770]
- Schmidt-Kastner R, Szymas J, Hossmann KA. Immunohistochemical study of glial reaction and serum–protein extravasation in relation to neuronal damage in rat hippocampus after ischemia. *Neuroscience.* 1990; 38:527–540. [PubMed: 1702195]
- Siesjo BK, Hu B, Kristian T. Is the cell death pathway triggered by the mitochondrion or the endoplasmic reticulum? *J Cereb Blood Flow Metab.* 1999; 19:19–26. [PubMed: 9886351]
- Silva AC, Lee JH, Aoki I, Koretsky AP. Manganese-enhanced magnetic resonance imaging (MEMRI): methodological and practical considerations. *NMR Biomed.* 2004; 17:532–543. [PubMed: 15617052]
- Sloot WN, Gramsbergen JB. Axonal transport of manganese and its relevance to selective neurotoxicity in the rat basal ganglia. *Brain Res.* 1994; 657:124–132. [PubMed: 7820609]
- Sofroniew MV. Reactive astrocytes in neural repair and protection. *Neuroscientist.* 2005; 11:400–407. [PubMed: 16151042]
- Sugaya K, Chouinard ML, McKinney M. Induction of manganese superoxide dismutase in BV-2 microglial cells. *NeuroReport.* 1997; 8:3547–3551. [PubMed: 9427324]
- Tiffany-Castiglioni E, Qian Y. Astroglia as metal depots: molecular mechanisms for metal accumulation, storage and release. *Neurotoxicology.* 2001; 22:577–592. [PubMed: 11770879]
- Watanabe T, Natt O, Boretius S, Frahm J, Michaelis T. *In vivo* 3D MRI staining of mouse brain after subcutaneous application of MnCl₂. *Magn Reson Med.* 2002; 48:852–859. [PubMed: 12418000]
- Wedler FC, Denman RB. Glutamine synthetase: the major Mn(II) enzyme in mammalian brain. *Curr Top Cell Regul.* 1984; 24:153–169. [PubMed: 6149889]
- Wideroe M, Olsen O, Pedersen TB, Goa PE, Kavelaars A, Heijnen C, Skranes J, Brubakk AM, Brekken C. Manganese-enhanced magnetic resonance imaging of hypoxic-ischemic brain injury in the neonatal rat. *NeuroImage.* 2009; 45:880–890. [PubMed: 19138750]
- Yang J, Wu EX. Detection of cortical gray matter lesion in the late phase of mild hypoxic-ischemic injury by manganese-enhanced MRI. *NeuroImage.* 2008; 39:669–679. [PubMed: 17949999]

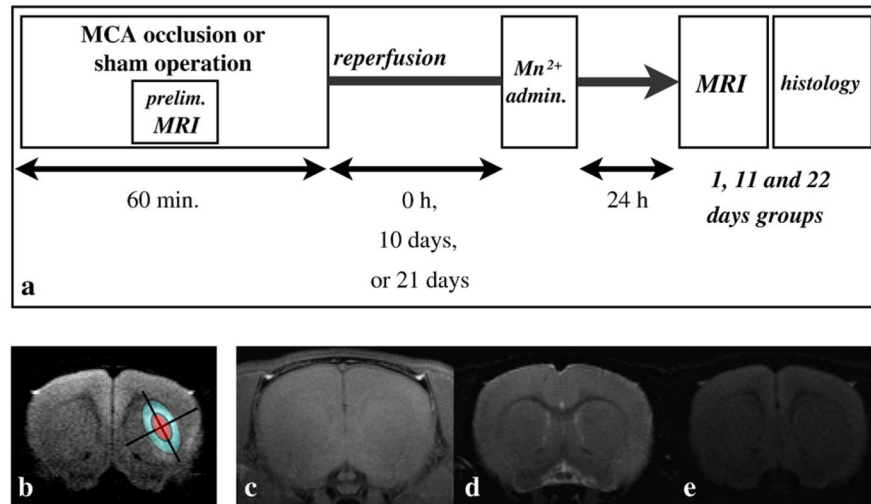


Fig. 1. Experimental procedure, ROI definition, and MRI in the sham model. (a) The middle cerebral artery was occluded for 60 minutes for the three MCAO groups. During the MCAO or sham operation, diffusion-weighted MRI and MR angiography were acquired to check whether the occlusion was successful. MnCl₂ solution was administered immediately after MCA reperfusion for the day 1 groups, 10 days after reperfusion for the day 11 groups, and 21 days after the reperfusion for the day 22 groups. MRI measurements were performed exactly 24 hours after the MnCl₂ administration for all groups. Finally, perfusion fixation and brain extraction were executed for immunohistochemical staining. (b) The ischemic core was determined as the small ellipse having major and minor axes half the length of the fitted ellipse (red region), and the ischemic periphery was determined as the region remaining after removing the ischemic core from the fitted ellipse (blue region). (c) Typical T₁-weighted manganese-enhanced MRI (MEMRI), (d) T₂-, and (e) diffusion-weighted MRI. No unilateral signal change was observed for any of the sham groups.

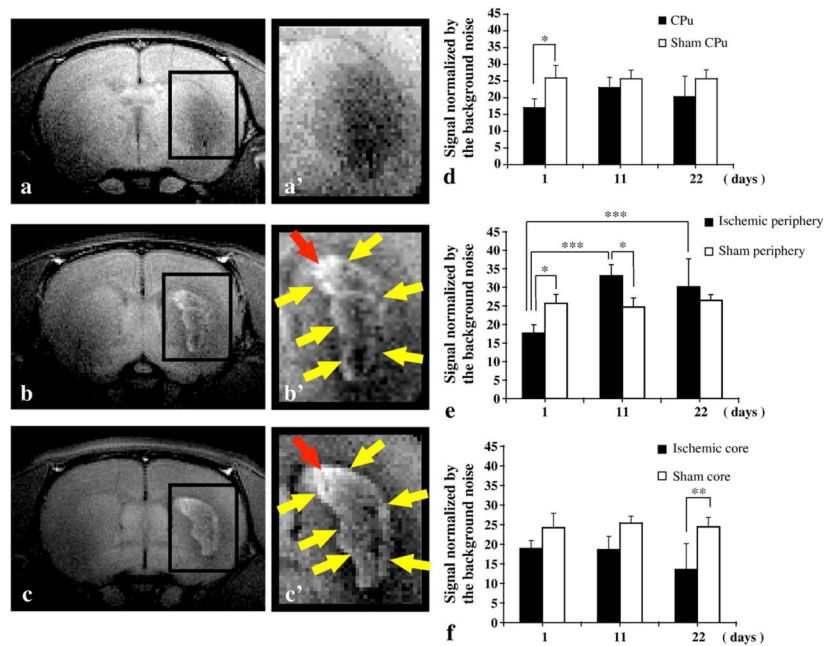


Fig. 2.

Longitudinal observation of manganese-enhanced MRI after MCAO. (a) Typical MEMRI 1 day after MCAO (day 1 group), and (a') magnification of the CPu where significant signal reduction was observed in comparison with the contralateral and unaffected brain tissues. (b) Typical MEMRI 11 days after MCAO (day 11 group) and (b') magnification of the CPu. Ring- or crescent-shaped enhancement was observed surrounding the ischemic core (yellow and red arrows). (c) Typical MEMRI 22 days after MCAO (day 22 group) and (c') magnification of the CPu. The ring- or crescent-shaped enhancement surrounding the ischemic core (yellow and red arrows) persisted, although the Mn-related enhancement of contralateral and unaffected tissues largely disappeared at this time. The highest signal intensity was observed in the region between the lateral ventricle and ischemic region (red arrows). (d) Comparison of normalized MEMRI signal across the entire CPu for the MCAO and sham groups. Significant signal reduction was observed for the day 1 after MCAO group in comparison with the sham group ($*p < 0.05$). No statistical differences were observed between the MCAO and sham conditions for the day 11 and day 22 groups. (e) Comparison of normalized MEMRI signal at the ischemic periphery for the MCAO and sham groups. Significant signal reduction was observed for the day 1 after MCAO group in comparison with the sham group ($*p < 0.05$). Significant signal increments were also observed for the day 11 after MCAO group when compared to the sham group ($*p < 0.05$) and the day 1 after MCAO group ($***p < 0.001$). The enhancement was also presented when the day 22 group was compared with the day 1 group ($***p < 0.001$). (f) Comparison of normalized MEMRI signal in the ischemic core for the MCAO and sham groups. Significant signal reduction was observed in the day 22 after MCAO group in comparison with the sham group ($**p < 0.01$). A tendency towards signal reduction in the core was also observed for the day 1 and day 11 after MCAO groups, although the differences were not statistically significant.

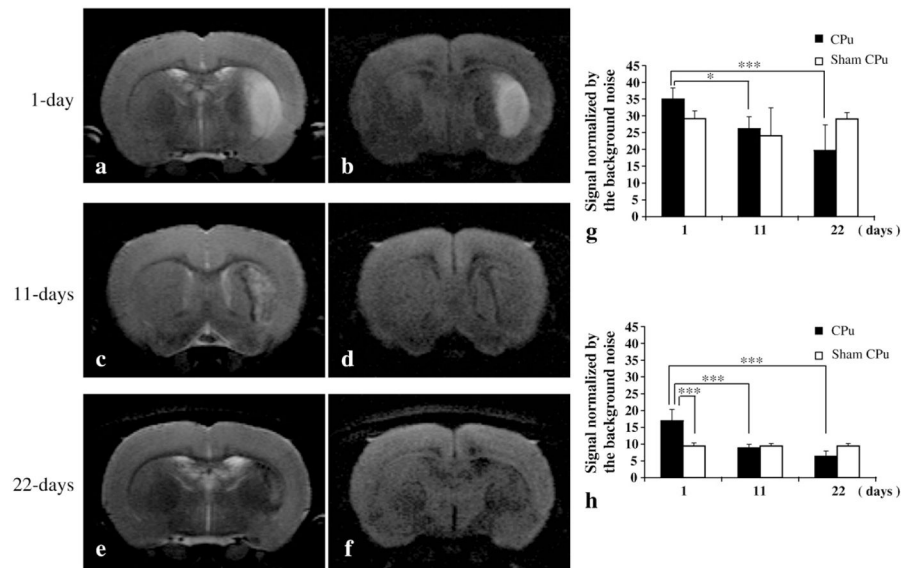


Fig. 3. Longitudinal observation of T₂ and diffusion-weighted MRI after MCAO. (a) T₂- and (b) diffusion-weighted MRI from the same day 1 after MCAO animal shown in Fig. 2a, a'. Significant signal enhancement was typically observed at the center and lateral side of the caudate putamen. A part of the ventral side of the cortex was also enhanced in some cases. The enhanced regions on both the T₂- and diffusion-weighted MRI corresponded to the signal-reduced area in the MEMRI. (c) T₂- and (d) diffusion-weighted MRI for the same day 11 after MCAO animal shown in Fig. 2b, b'. Maculate and feeble signal enhancement was observed on the lateral side of the CPu in the T₂-weighted MRI (c). No signal enhancement was observed on the diffusion-weighted MRI (d). Signal reduction corresponding to the MEMRI ring-shaped signal enhancement was observed on both the T₂- and diffusion-weighted MRI for the day 11 group (c and d). (e) T₂- and (f) diffusion-weighted MRI for the same day 22 after MCAO animal shown in Fig. 2c, c'. (g) Comparison of the normalized T₂-weighted MRI in the CPu for the MCAO and sham groups. Significant signal enhancement was observed for the day 1 after MCAO group (***) $p < 0.001$, ** $p < 0.05$), but this had returned to the original level for the day 11 after MCAO group. (h) Comparison of the normalized diffusion-weighted MRI in the CPu for the MCAO and sham groups. Significant signal enhancement observed for the day 1 after MCAO group (***) $p < 0.001$) had returned to the same level as the sham group for the day 11 and day 22 after MCAO groups.

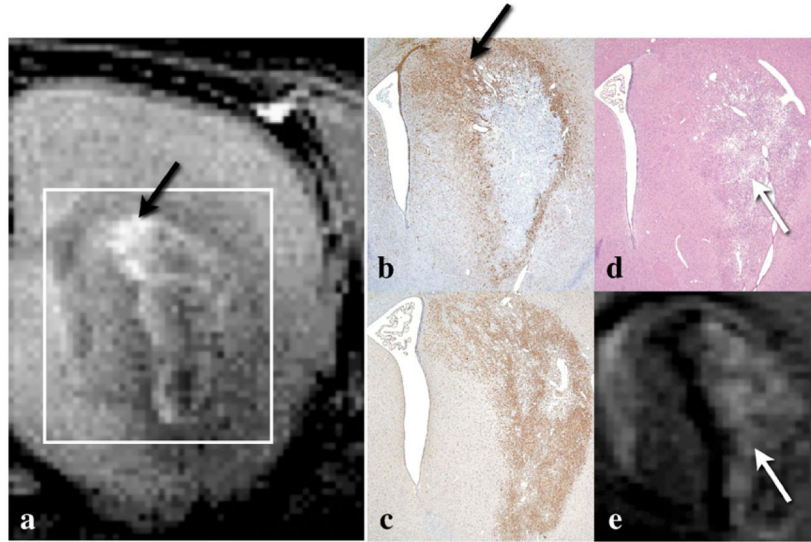
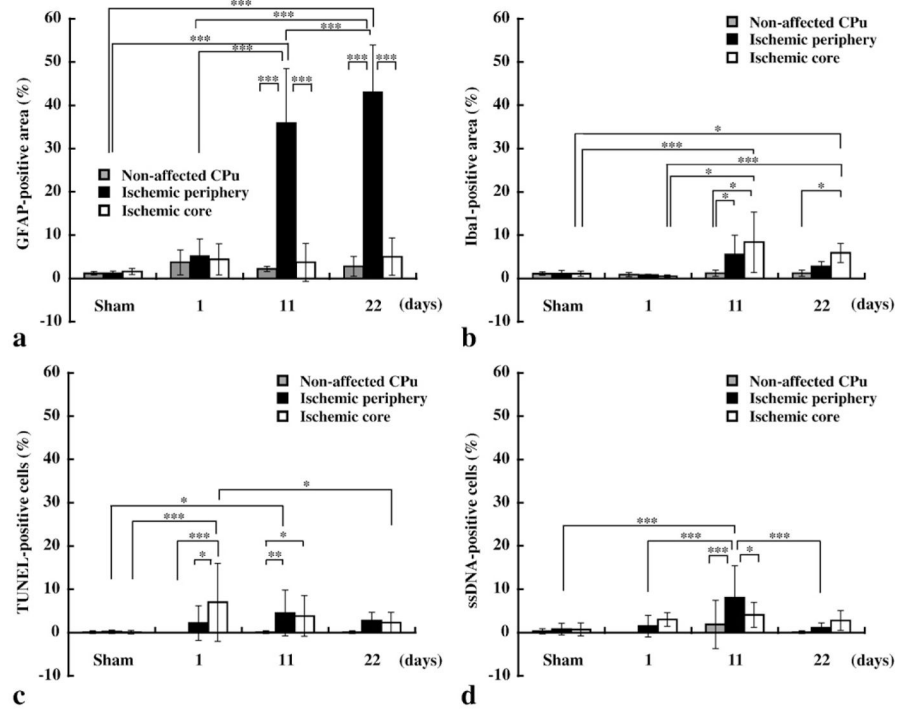


Fig. 4. Comparison of MEMRI and immunohistochemical staining. Typical (a) MEMRI, (b) GFAP, (c) Iba1, (d) HE staining, and (e) T₂-weighted MRI from the same animal in the day 11 after MCAO group as shown in Figs. 2a, a' and 3c and d. Ring- or crescent-shaped enhancement on the MEMRI (a) agreed well with the GFAP-positive region (b). The highest density of GFAP-positive cells was observed in the area between the lateral ventricle and ischemic region (b, black arrow) in agreement with the MEMRI (a, black arrow). Agreement among the MEMRI (a), Iba1 (c), and HE (d) stainings was not found. Iba1-positive cells were distributed throughout the entire ischemic region (c), similar to the distribution in the necrotic region shown by the HE staining (d, white arrow) and T₂-weighted MRI (e, white arrow).

**Fig. 5.**

Evaluation of immunohistochemical stainings. Gray, black, and white bars indicate areas in non-affected CPu, ischemic periphery, and core, respectively (see also Fig. 7 for the ROI definitions). (a) Comparison of the ratio of the GFAP-positive cell area-to-total area. (b) Comparison of the ratio of the Iba1-positive cell area-to-total area. (c) Comparison of the ratio of the number of TUNEL-positive cells to the total number of cells. (d) Comparison of the ratio of the number of ssDNA-positive cells to the total number of cells. Level of significance: * $P < 0.05$, ** $P < 0.001$, and *** $P < 0.0001$ for Tukey's multiple comparison test.

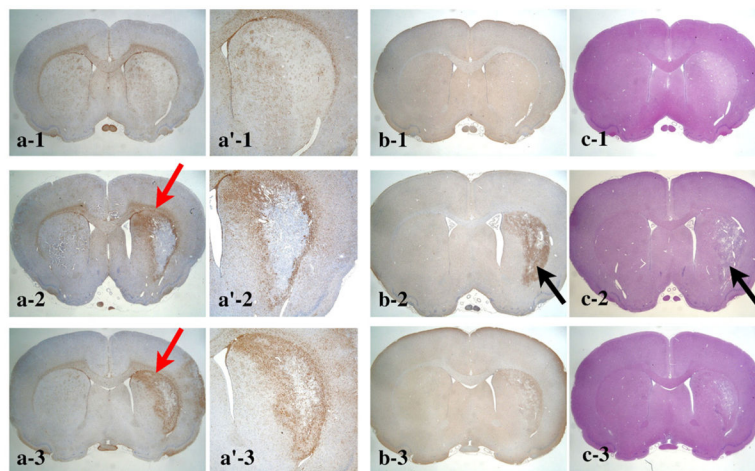


Fig. 6. Longitudinal observation of immunohistochemical staining. Typical (a) GFAP ((a') magnification of GFAP), (b) Iba1, and (c) HE staining are presented for the day 11 after MCAO group. The animal shown in panels a-1, b-1, and c-1 for the day 1 group is the same as that shown in Figs. 2a and 3a, b. Similarly, the animal in panels a-2, b-2, and c-2 for the day 11 group is the same as that shown in Figs. 2b and 3c and d. Moreover, the histology shown in panels a-3, b-3, and c-3 was from the same animal in the day 22 group as shown in Figs. 2c and 3e and f. No unilateral increment of cells was observed for the GFAP (a-1 and a'-1), Iba1-positive cells (b-1), or HE staining (c-1) of the day 1 after MCAO group. Slight reductions of Iba1-positive and eosin staining were observed in the affected CPu (a-1 and c-1) corresponding to the signal enhancement in the T_2 - and diffusion-weighted MRI (Figs. 3a and b). The ring- or crescent-shaped GFAP-positive cells surrounding the ischemic core were clearly observed for the day 11 group (a-2, a'-2, red arrow). Iba1-positive cells were distributed throughout the necrotic ischemic core 11 days after MCAO (b-2 and c-2, black arrows). A similar ring- or crescent-shaped distribution of proliferated GFAP-positive cells was observed for the day 22 after MCAO group (a-3, red arrow). The number of Iba1-positive cells in the ischemic core decreased for the day 22 after MCAO group in comparison to the day 11 group (b-3).

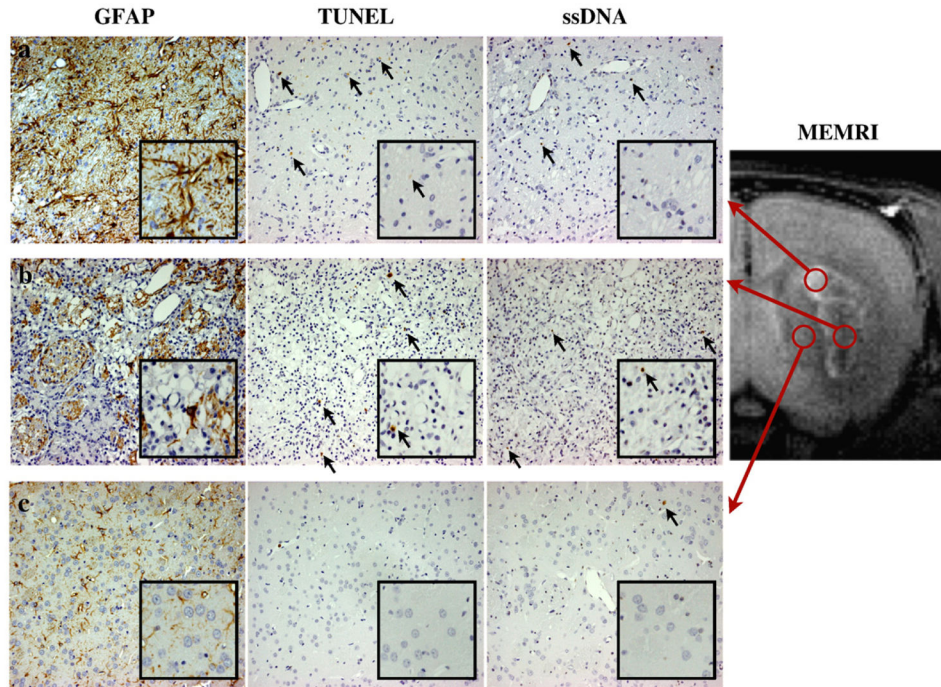


Fig. 7. Evaluation of apoptosis using TUNEL and ssDNA immunohistochemical stainings. From left to right, the three columns show the results of GFAP, TUNEL, and ssDNA stainings at a magnification of 200 \times for the day 11 after MCAO group. The inset in the lower right corner of each image is a digital magnification. (a) The images in the upper row were observed in the ischemic periphery corresponding to the signal-enhanced area in the MEMRI (upper red circle). Most of the tissue was replaced by GFAP-positive astroglia. Although TUNEL- and ssDNA-positive cells were also observed in this region (a, black arrows), the density of the positive cells was low (see also Figs. 5c and d). (b) The middle row displays the histology for the ischemic core. Tissue deficit and pyknomorphous cells were observed for all stainings. GFAP-positive astroglia were also observed, although the density was much lower than for the ischemic periphery. (c) The bottom row presents histology corresponding to the nonenhanced part of the CPU in the MEMRI. Few GFAP-positive cells were observed in this region. Also, TUNEL- and ssDNA-positive and pyknomorphous cells were sparse.

Table 1

Animal physiology.

| | Blood pCO ₂ before operation (mm Hg) | Blood pO ₂ before operation (mm Hg) | Blood pH before operation |
|-------------|---|--|---|
| MCAO groups | 33.2±3.4 | 101.0±13.5 | 7.42±0.03 |
| Sham groups | 33.6±0.8 | 91.5±16.2 | 7.45±0.03 |
| | | Body temperature before MCAO (°C) | Body temperature after reperfusion (°C) |
| MCAO groups | 1 day | 37.1±0.1 | 38.2±0.7 |
| | 11 days | 38.1±0.3 | 37.9±0.3 |
| | 22 days | 37.7±0.2 | 37.2±0.5 |
| Sham groups | 1 day | 37.6±0.5 | 37.4±0.4 |
| | 11 days | 37.4±0.1 | 37.0±1.3 |
| | 22 days | 37.4±0.5 | 37.2±0.6 |

The arterial blood gas parameters, including carbon dioxide partial pressure (pCO₂), oxygen partial pressure (pO₂) and pH, were maintained within normal physiological ranges before both the MCAO and sham operations. No significant statistical differences were observed between the MCAO and sham-operated groups ($P < 0.05$, unpaired T test). Body temperature was also maintained within the normal physiological range for every group before and after the operations ($P < 0.05$, Tukey's multiple comparison test).